

Tailored Particle Beams From Single-Component Plasmas

T. R. Weber, J. R. Danielson and C. M. Surko

Department of Physics, University of California, San Diego, La Jolla CA 92093-0319

Abstract. Recently, we developed a non-destructive technique to create narrow beams of electrons (or positrons) of adjustable width and brightness from single-component plasmas confined in a Penning-Malmberg trap [Weber et al., Phys. Plasmas **13**, 123502 (2008)]. Here, we review highlights of that work and discuss the distributions in energy of the extracted beams. A simple model for beam extraction predicts Gaussian beam profiles, with transverse spatial widths dependent on the number of particles in the beam. A Maxwellian energy distribution is predicted for small beams. The predictions of the theory are confirmed using electron plasmas. Extraction of over 50% of a trapped plasma into a train of nearly identical beams is demonstrated. Finally, the possibility of creating high quality, electrostatic beams by extraction from the confining magnetic field is discussed.

Keywords: bright beams, narrow beams, positrons, antiprotons, antimatter, nonneutral plasmas.

PACS: 52.27.Jt, 52.35.-g, 34.80.Uv, 41.75.Fr, 41.85.Ar.

INTRODUCTION

Charged particle beams are used for a wide range of applications in science and technology. In the case of electrons, beams generated by a simple heated cathode or field emission are adequate for most applications. However, when the particles are more difficult to obtain, as is the case with positrons and antiprotons, for example, more refined techniques are required. In the case of antimatter, it has proven convenient to use trap-based beams, where the particles are first accumulated efficiently and cooled in an electromagnetic trap, then a beam or pulse of particles is extracted [1-4]. In this paper, we describe the use of a Penning-Malmberg trap to create high-quality, trap based beams, having in mind that this is directly relevant to the creation of state-of-the-art positron beams. These beams are extracted from the center of the single-component plasma by carefully lowering an end-gate confining potential. Much of this paper is an overview of recent work that is described in more detail elsewhere [5, 6].

Many applications require positron or antiproton beams with small transverse spatial extent and small energy spreads [4, 7-9]. We describe here techniques to create such beams with radii, ρ_b , as small as 10 μm and energy spreads of the order of the temperature of the parent plasma (i.e., which is cooled by cyclotron radiation in the confining, 5 T magnetic field). For rare particles, such as positrons, it is advantageous to use them efficiently. As discussed below, that can be done with near 100% efficiency using the techniques described here.

Penning-Malmberg Trap for Beam Extraction

The plasma particles are accumulated and stored in a Penning-Malmberg trap, such as that shown schematically in Fig. 1 (a) [6]. It consists of a set of cylindrical electrodes, of radius $R_W = 1.2$ cm, in a uniform magnetic field of strength $B = 5$ T. The particles are confined radially by the magnetic field and axially by voltages, V_C applied to electrodes at each end. The resulting plasma is in thermal equilibrium at temperature T . The plasma is a uniform-density rigid rotor, rotating at an $E \times B$ frequency, $f_E = cn_0e/B$, proportional to the equilibrium density, n_0 . The plasma parameters are z -independent, thus making r and θ the coordinates of interest.

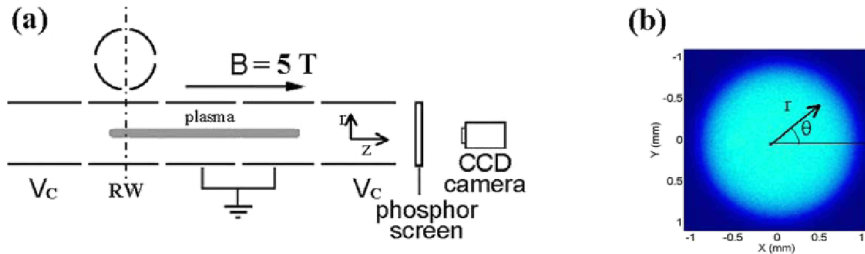


FIGURE 1. (a) Schematic diagram of the experimental arrangement; and (b) a CCD images of the areal plasma density, $\sigma_z(r, \theta)$, for an equilibrium, “flat-top” plasma.

The principal diagnostic used here is imaging the two-dimensional (i.e., areal) plasma density using a phosphor screen located outside the trap and a CCD camera. By quickly setting $V_C = 0$ at one end of the plasma, the plasma particles stream out of the trap along the magnetic field. They are accelerated to energies of 5 keV, and then collide with the phosphor screen. The resulting fluorescent light is imaged with a CCD camera to obtain the z -integrated, areal plasma density profile, $\sigma_z(r, \theta)$. A typical CCD image is shown in Fig. 1 (b). The plasma density, n , is then $n(r, \theta) = \sigma_z / L_P$, where L_P is the plasma length.

Another important technique for the work described here is use of rotating electric fields to compress the plasma radially [i.e., the so-called “rotating wall” (RW) technique] [10]. The segmented electrode for this is shown in Fig. 1 (a). Phased, sinusoidal voltages are applied to each of the four segments. This azimuthally asymmetric potential rotates around the z -axis, hence the name “rotating wall”. For sufficiently large sine wave voltages, the plasma spins up (or down) to the applied RW frequency, f_{RW} [10]. Because f_E is proportional to the equilibrium density, n_0 , the plasma density can thus be set, *in situ*, in a non-destructive way, by simply tuning f_{RW} .

BEAM EXTRACTION

To extract a beam from a trapped plasma, the confining potential, V_C , at one end of the plasma is lowered to a value V_E for about 15 μ sec. This time is chosen to be sufficiently long so that particles with sufficient energy have enough time to escape, but short enough so that instabilities and radial transport are negligible. This process is

illustrated schematically in Fig. 2 (a). Because the plasma potential is highest at the (radial) center of the plasma, the beam is composed of particles from this region. This is highly beneficial, as it creates beams with spatial extent much smaller than that of the parent plasma. Fig. 2 (b) shows CCD images of a plasma before and after a beam is extracted. Notice the small hole at the center, illustrating the location of the particles that exited the trap.

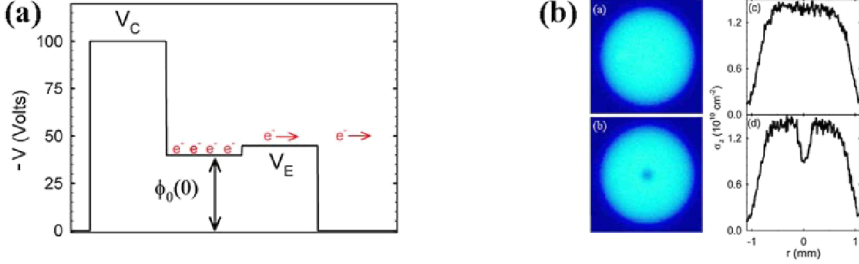


FIGURE 2. (a) Schematic diagram of the beam extraction process. (b) CCD camera images of the areal plasma density, profile, $\sigma_z(r, \theta)$ for a “flat top” plasma before, and 10 μ s after, beam extraction; also shown are the corresponding (slice) distributions, $\sigma_z(r)$.

THEORETICAL CONSIDERATIONS

When the end-gate potential is lowered to V_C , particles will begin to escape. As they do, the space-charge potential near the center of the plasma will change in such a way as to inhibit further particles from leaving. The condition that particles escape will be

$$E \geq E_{MIN} = -e(V_E - \phi_0(r) + \Delta\phi(r)), \quad (1)$$

where E_{MIN} is the energy required for a particle to escape at the end of the beam extraction, $\phi_0(r)$ is the equilibrium plasma potential and hence is quadratic in r , and $\Delta\phi(r)$ is the change in the plasma potential due to the extracted beam particles. After extraction, the new density and space-charge potential profiles are $n(r) = n_0(r) - \Delta n(r)$, and $\phi(r) = \phi_0(r) - \Delta\phi(r)$.

The areal density profile, $\sigma_b(r)$, as measured using the phosphor screen, will be $\sigma_b(r) = \Delta n(r) \times L_P$. Assuming an initially uniform density plasma in thermal equilibrium, $\sigma_b(r)$ can be written

$$\sigma_b(r) = 2n_0L_P \int_{E_{MIN}}^{\infty} f(E_{\parallel})dE_{\parallel} = 2L_P n_0 \text{erfc} \left(\sqrt{-\frac{e}{T}(V_E - \phi_0(r) + \Delta\phi_0(r))} \right). \quad (2)$$

Assuming E_{MIN} is on the tail of the Maxwellian, $\text{erfc}(x) \sim \exp(-x^2)/x$. Then approximating $\Delta\phi(r)$ as the change in potential due to a “flat top” beam of width, ρ_b , and using the expression for $\phi_0(r)$ [6],

$$\sigma_b(r) = \sigma_{b0} \exp\left[-\left(\frac{r}{2\lambda_D}\right)^2 + \xi\left(\frac{r}{\rho_b}\right)^2\right], \quad \text{where } \xi = \frac{e^2 N_b}{L_p T}. \quad (3)$$

Here, σ_{b0} is a function of V_E and approximately constant for all r . Defining ρ_b as the half width to $1/e$, this width becomes,

$$\rho_b = 2\lambda_D(1 + \xi)^{1/2} \quad (4)$$

The quantity ξ is the key parameter that determines the size of extracted beams. For small values of ξ , Eq. (3) predicts a Gaussian beam with a full width to $1/e$ of $4\lambda_D$.

A key quantity of interest is the distribution of beam particles in parallel energy space, $f(E_{\parallel})$, which is defined as dN_b/dV_E , evaluated at $V_E = E_{\parallel}$. From Eq. 3, it can be seen that $\sigma_{b0} \sim N_b$. In the limit of small beams (i.e., $\xi \ll 1$), $e\Delta\phi/T$ can be neglected in Eq. (2), so that

$$\left. \frac{d\sigma_{b0}}{dV_E} \right|_{V_E=E_{\parallel}} \propto f(E_{\parallel}) \propto \frac{\exp[-(E_{\parallel} - e\phi_0(0))/T]}{\sqrt{(E_{\parallel} - e\phi_0(0))/T}}. \quad (5)$$

Equation (6) is just the tail of the energy distribution of a Maxwellian sitting at an electrical potential of $\phi_0(0)$. Thus, for small beams, the parallel energy spread is $\sim T$.

SINGLE BEAMS

Shown in Fig. 3 (a) are areal density profiles for beams of different amplitudes. The corresponding beam widths as a function of ξ are shown in Fig. 3 (b). The results of the previous section predict Gaussian beam profiles for small beams with a full width

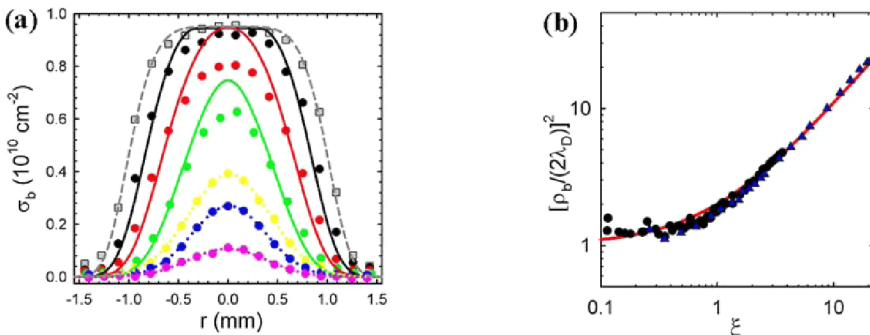


FIGURE 3. (a): Profiles, $\sigma_b(r)$, of extracted beams from a $T = 1.0$ eV plasma with density, $n_0 \approx 1 \times 10^9$ cm^{-3} . From smallest to largest, $\xi \approx 0.1, 0.3, 0.5, 1.0, 1.9, 2.8$ for each beam. The three smallest beams are fit (\cdots) to Eq. 3. The initial plasma profile, $\sigma_z(r)$, (\blacksquare) is also shown. (b): Beam width parameter, ρ_b , plotted vs. ξ for $T = 1.0$ eV (\bullet), and 0.2 eV (\blacktriangle). The prediction (---) from Eq. 4, with no fitted parameters, is also shown.

to $1/e$ of $4\lambda_D$, and the data in Fig 3 are in agreement with this prediction. The predictions of Eq. 4 are valid for all values of ξ tested, while the Gaussian profile predicted in Eq. 3 is valid for $\xi < 1$ (c.f., Fig. 3). The solid lines in Fig. 3 (a) are the results of numerical calculations for larger beams; see Ref. [6] for details.

Shown in Fig. 4 are the radial profiles of beams extracted before and after RW compression of the parent plasma. These data illustrate the ability to create, nondestructively, beams with narrow transverse spatial extent and thus enhanced brightness. For the beam shown in Fig 4 (b), the beam brightness was increased by a factor of 40, while ξ remains constant.

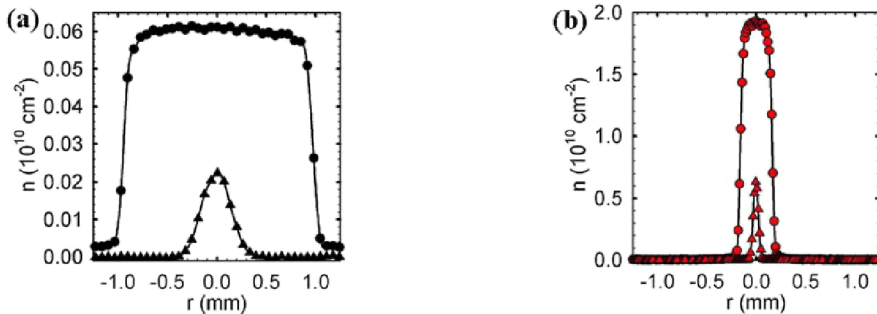


FIGURE 4. Beams with $\xi = 0.5$, extracted from a plasma (a) before RW compression, with $n_0 \approx 0.6 \times 10^9 \text{ cm}^{-3}$; and (b) after RW compression, with $n_0 \approx 20 \times 10^9 \text{ cm}^{-3}$. In both cases, $T = 0.05 \text{ eV}$.

The parallel energy distributions of two extracted beams are shown in Fig. 5. As shown in Fig. 5 (a), for the smallest beam, with $\xi = 0.02$, the predictions of Eq. (5) are in excellent agreement with the data. However, as shown in Fig. 5 (b), when ξ is increased to the seemingly still small value of 0.1, the predictions of Eq. (5) deviate significantly from the data. The resulting beam energy distributions for larger beams, the shifts in mean beam energy and energy spread are due to the non-negligible effects of $\Delta\phi(r)$ and will be discussed elsewhere.

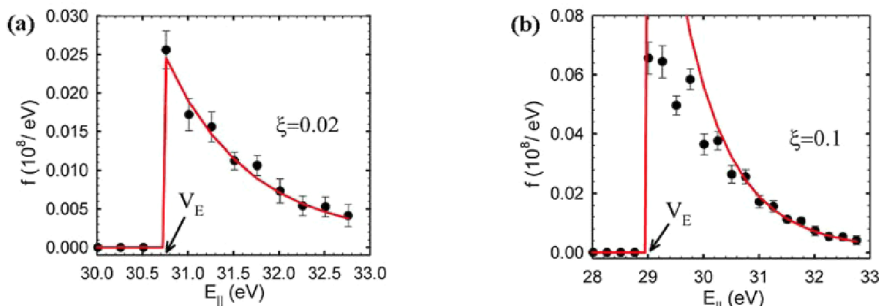


FIGURE 5. Energy distributions of beams extracted from a plasma with $T = 1.0 \text{ eV}$, $n_0 \approx 1 \times 10^9 \text{ cm}^{-3}$ for (a) $\xi = 0.02$, and (b) $\xi = 0.1$. Also shown are the predictions of Eq. 6 (—), for $\phi_0(0) = 28 \text{ V}$.

EXTRACTION OF MULTIPLE BEAMS

Due to the relative scarcity of positrons, it is desirable to use them as efficiently as possible. Data for such an efficient extraction from an electron plasma are shown in Fig. 6 where 20 nearly identical beams were extracted utilizing over 50 % of the parent plasma with essentially no loss of particles. The beams were extracted serially, waiting for the plasma to recover to its equilibrium state [i.e., from a state such as that shown in Fig. 2 (b)], then pulsing V_C to another value of V_E which was carefully chosen to maintain constant N_b . The plasma recovers in ~ 0.5 ms via an unstable diocotron mode [11]. Care was taken to ensure that the plasma relaxes to thermal equilibrium, which is expected to occur on a shorter time scale (i.e., $\tau_{ee} < 0.5$ msec) [6]. During extractions, the RW is kept on to maintain constant n_0 , thus fixing λ_D and ρ_b . The nearly identical nature of the radial beam profiles is illustrated in Fig. 6 (b).

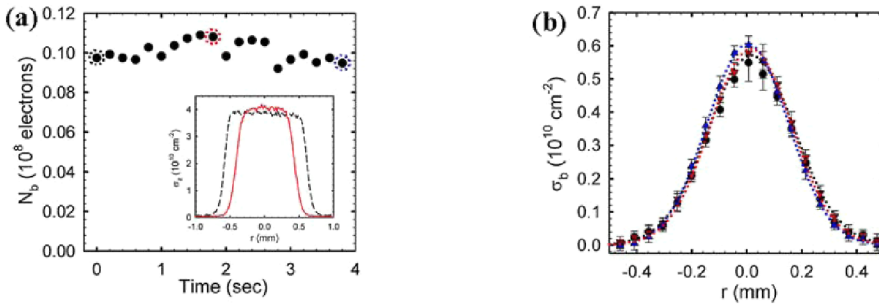


FIGURE 6. (a) N_b for twenty beams extracted consecutively from the same plasma with $T \approx 0.3$ eV and $n_0 \approx 2 \times 10^9$ cm $^{-3}$. Here, $\langle N_b \rangle = 0.1 \pm 0.005 \times 10^8$ and $\xi \approx 0.2$. The inset shows the radial profiles, $\sigma_z(r)$, of the plasma before (---) and after (—) extraction of the 20 beams. (b) radial beam profiles, $\sigma_b(r)$, for the 1st (●), 10th (▲), and 20th (▼) beam pulse.

ELECTROSTATIC BEAMS

For some applications, pulses of positrons are desired in a magnetic-field-free region (e.g., to accommodate electrostatic focusing techniques) [12]. This can be accomplished by pulling the particles out of the field in a non-adiabatic manner. However, for the 5 T field used here, this would require the magnetic field to drop to zero in distances < 100 μm , which would be difficult to achieve experimentally. Thus we propose extracting the particles from the field in two stages: Stage I, a slow adiabatic reduction of B along the beam path from 5 T to 0.5 mT; then Stage II, a rapid non-adiabatic extraction from $B = 0.5$ mT to zero. In Stage I, the field will be decreased over large distances so that the particles remain on field lines while the adiabatic invariant, $E_{\perp}/|B|$ is conserved. This has the effect of cooling the perpendicular temperature, T_{\perp} , while the beam expands spatially due to the diverging field lines. To conserve energy, T_{\parallel} increases accordingly.

In the non-adiabatic stage, the particles are removed from the field lines, receiving an impulse in the azimuthal direction to conserve canonical angular momentum. This

results in an increase in E_{\perp} with a corresponding decrease in E_{\parallel} . This kick is dependent upon r , so the finite spatial extent of the beam results in an increased spread in T_{\perp} and T_{\parallel} . Table I summarizes the predicted beam parameters for a parent plasma with $n_0 \approx 1 \times 10^{10} \text{ cm}^{-3}$ and $T = 30 \text{ K}$ (i.e., $\approx 3 \text{ meV}$) that could be created with cryogenically cooled electrodes. While the beam width has increased by a factor of 100, and T_{\perp} by a factor of 3, such a positron beam would be of excellent quality for a variety of applications, including positron-atomic physics and the characterization of materials.

Table I. Parameters for the creation of positron pulses in a magnetic, field-free region, starting with (I) an initial pulse in a 5 T field; (II) adiabatic transfer to a field of 0.5 mT; and then (III) non-adiabatic extraction from the field.

PARAMETER	STAGE I	STAGE II	STAGE III
B (Tesla)	5	5×10^{-4}	0
T_{\perp} (meV)	3	6	9
T_{\parallel} (meV)	3	3×10^{-4}	3
ρ_b (cm)	5×10^{-4}	5×10^{-2}	5×10^{-2}

CONCLUSION

Described here is a method to extract beams of tailored width and brightness in a non-destructive, reproducible manner from plasmas in a Penning-Malmberg trap. A formalism is described that predicts the beam width and energy spread, namely the key parameters of interest for a range of applications. The ability to extract multiple, nearly identical beams is demonstrated, utilizing over 50 % of a single trapped plasma with no loss of particles. Finally, a scenario is discussed in which the techniques described here can be used to produce high-quality electrostatic beams that are expected to be useful for a variety of positron applications.

ACKNOWLEDGMENTS

We wish to acknowledge helpful conversations with R. G. Greaves and the expert technical assistance of E. A. Jerzewski. This work was supported by the NSF, Grant Nos. PHY-03-54653 and PHY 07-13958.

REFERENCES

1. S. J. Gilbert, C. Kurz, R. G. Greaves, and C. M. Surko, *Appl. Phys. Lett.* **70**, 1944 (1997).
2. C. Kurz, S. J. Gilbert, R. G. Greaves, and C. M. Surko, *Nucl. Instrum. Methods in Phys. Res.* **B143**, 188 (1998).
3. D. B. Cassidy, S. H. M. Deng, R. G. Greaves, and A. P. Mills, Jr., *Rev. Sci. Instrum.* **77**, 073106 (2006).
4. C. M. Surko and R. G. Greaves, *Phys. Plasmas* **11**, 2333 (2004).
5. J. R. Danielson, T. R. Weber, and C. M. Surko, *Appl. Phys. Lett.* **90**, 081503 (2007).
6. T. R. Weber, J. R. Danielson, and C. M. Surko, *Phys. Plasmas* **13**, 123502 (2008).
7. D. B. Cassidy and A. P. Mills, Jr., *Nature* **449**, 195 (2007).
8. M. Amoretti, C. Amsler, G. Bonomi, A. Bouchta, P. Bowe, C. Carraro, C. L. Cesar, M. Charlton, M. Collier, M. Doser, V. Filippini, K. Fine, A. Fontana, M. Fujiwara, R. Funakoshi, P. Genova, J. Hangst, R. Hayano, M. Holzschetter, L. Jorgensen, V. Lagomarsino, R. Landua, D. Lindelof, E. L. Rizzini, M. Macri, N. Madsen, G. Munuzio, M. Marchesotti, P. Montagna, H. Pruys, C. Regenfus, P. Riedler, J.

- Rochet, A. Rotondi, G. Rouleau, G. Testera, A. Variola, T. Watson, and D. VanderWerf, *Nature* **419**, 456 (2002).
9. G. Gabrielse, N. Bowden, P. Oxley, A. Speck, C. Storry, J. Tan, M. Wessels, D. Grzonka, W. Oelert, G. Schepers, T. Seifzick, J. Walz, H. Pittner, T. Hansch, and E. Hessels, *Phys. Rev. Lett.* **89**, 213401 (2002).
 10. J. R. Danielson and C. M. Surko, in *Non-Neutral Plasma Physics VI*, edited by M. Drewsen, U. Uggerhoj and H. Knudsen (American Institute of Physics Press, 2006), p. 19
 11. C. F. Driscoll, *Phys. Rev. Lett.* **64**, 645 (1990).
 12. C. M. Surko, G. F. Gribakin, and S. J. Buckman, *J. Phys. B: At. Mol. Opt. Phys.* **38**, R57 (2005).